Lifetime Extension Approach Based on the Levenberg–Marquardt Neural Network and Power Routing of DC–DC Converters

Jiusi Zhang, *Student Member, IEEE*, Jilun Tian, *Student Member, IEEE*, Abraham M. Alcaide, *Member, IEEE*, Jose I. Leon, *Fellow, IEEE*, Sergio Vazquez, *Fellow, IEEE*, Leopoldo G. Franquelo, *Life Fellow, IEEE*, Hao Luo, *Senior Member, IEEE*, and Shen Yin, *Fellow, IEEE*

***Abstract*—The power conversion system based on the modular connection has widespread applications in various power electronic systems. To accurately estimate the state of health without recognizing the systematic mathematical model and to extend the lifetime, this article proposes a lifetime extension approach based on the Levenberg–Marquardt back propagation neural network (LM-BPNN) and power routing of interleaved dc–dc boost conversion systems. The LM-BPNN model is constructed based on the voltage, current, and temperature data generated by the system. On the basis of the trained LM-BPNN, the real-time cumulated damage estimation of each power cell in the conversion system can be accomplished. Applying the power routing concept, the dc–dc boost conversion system allocates different power to the cells according to the cumulated damage of each cell, thereby delaying the failure of cells with higher cumulated damage. Numerical simulation results show that the proposed lifetime extension approach can extend the overall system lifetime. Furthermore, an experimental setup of the interleaved dc–dc boost conversion is constructed to verify the proposed approach, which is of great significance for predictive maintenance in the industrial system.**

Manuscript received 11 January 2023; revised 16 March 2023; accepted 3 May 2023. Date of publication 12 May 2023; date of current version 21 June 2023. This work was supported in part by the National Natural Science Foundation of China under Grant 62073104. The work of A. M. Alcaide, J. I. Leon, S. Vazquez, and L. G. Franquelo was supported in part by the Project PID2020-115561RB-C31 funded by MCIN/AEI/10.13039/501100011033, in part by the Project TED2021-130613B-I00 funded by MCIN/AEI/10.13039/501100011033, and in part by the "European Union NextGenerationEU/PRTR." The work of A. M. Alcaide was supported in part by Contratación de Personal Investigador Doctor, in part by Convocatoria 2019, 43 Contratos Capital Humano Línea 2, and in part by El Plan Andaluz de Investigación, Desarrollo e Innovación (PAIDI) 2020, supported by the European Social Fund and Junta de Andalucía. Recommended for publication by Associate Editor H. Wang. *(Corresponding author: Hao Luo.)*

Jiusi Zhang, Jilun Tian, and Hao Luo are with the Department of Control Science and Engineering, Harbin Institute of Technology, Harbin 150001, China (e-mail: hit_zjs@163.com; jltian0208@163.com; hao.luo@hit.edu.cn).

Abraham M. Alcaide is with the Department of Electronic Engineering, School of Engineers, University of Seville, 41092 Seville, Spain (e-mail: amarquez@ieee.org).

Jose I. Leon, Sergio Vazquez, and Leopoldo G. Franquelo are with the Laboratory of Engineering for Energy and Environmental Sustainability, Universidad de Sevilla, 41092 Sevilla, Spain (e-mail: jileon@us.es; sergi@us.es; lgfranquelo@ieee.org).

Shen Yin is with the Department of Mechanical and Industrial Engineering, Faculty of Engineering, Norwegian University of Science and Technology, 7034 Trondheim, Norway (e-mail: shen.yin@ntnu.no).

Color versions of one or more figures in this article are available at https://doi.org/10.1109/TPEL.2023.3275791.

Digital Object Identifier 10.1109/TPEL.2023.3275791

***Index Terms*—Extension, interleaved dc–dc conversion system, Levenberg–Marquardt back propagation neural network (LM-BPNN), lifetime, power routing.**

I. Introduction

THE modern power systems have become more complex with large-scale structures, so the intelligent grids have gained more and more attention [1], [2], [3], [4], [5]. In the intelligent grid technology, new power converter topologies, advanced power device technologies, and control and modulation methods have become current research hotspots [6], [7], [8]. Due to these advances, the power converters can meet the demand for electric energy, which ensures the normal operation of the power grid [9], [10], [11], [12].

To face these requirements, using modular converters is an attractive solution. The power conversion system based on modular connection refers to connecting several power converters in series or parallel. The nominal power is usually equally shared among the different power cells [13], [14]. The power conversion systems based on the modular connection are widely used in various power electronic equipment ranging from low power to high power [15], [16]. As a typical power conversion system based on modular connection, the parallel dc–dc conversion system keeps the losses below acceptable levels by sharing the current among the power cells during the operation. As an example of parallel-connected dc–dc converters, Fig. 1 represents the electrical schematic of the Vensys 60/1200 commercial wind power generation system [17]. Each stage of the system adopts a parallel modular connection mode. The dc rectified voltage is generated according to the diode rectifier bridge, and is boosted by an interleaved boost dc–dc conversion system. Finally, the voltage is connected to the main grid through two parallel-connected two-level voltage source inverters.

During the operation of a power electronic system, power devices are influenced by the factors such as high thermal stress, power loss, and ambient temperature. Therefore, an accurate estimation of the state of health (SOH) of the power electronic systems in real time is required. This SOH estimation will help the system manufacturer improve the reliability and the fault-tolerant capability [18], [19], [20]. In [21], it is verified that the failure of power devices is mainly related to thermal stress

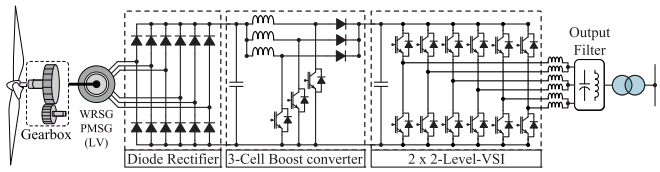

Fig. 1. Electrical schematic of the Vensys 60/1200 commercial wind power generation system.

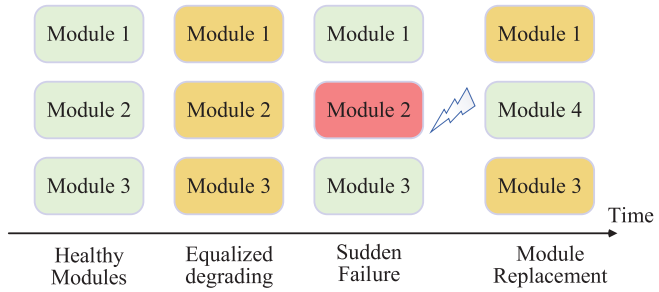

Fig. 2. Degrading evolution in a modular DC–DC conversion system considering replacements and failures.

caused by solder joint fatigue. Furthermore, repeated thermal cycles will cause irregular expansion and contraction of power device materials, thereby causing failure. The authors in [22] proposed adaptive joint extended Kalman filter and adaptive dual Kalman filter approaches to predict the remaining useful lifetime of the interleaved dc–dc boost conversion system used in electric vehicles.

In recent years, the application of artificial intelligence to reliability analysis of power electronics has attracted more and more attention. Zhao et al. [23] processed an in-depth overview of the design, control, and maintenance of power electronics with the aid of artificial intelligence approaches. Considering the nonlinear electronics thermal characteristics of power devices, Chiozzi et al. [24] proposed a neural network (NN)-based modeling approach for power devices, which is helpful to reproduce circuit conditions. Facing the uncertainty of life estimation, Eleffendi et al. [25] proposed an online approach based on the Kalman filter and recursive least squares to monitor key semiconductor parameters, to achieve predictive maintenance.

In the conventional interleaved boost dc–dc conversion system, each converter cell manages the same power by applying an equalized current sharing control strategy. In this way, assuming ideal conditions, the power loss, thermomechanical fatigue, and cumulative aging of each power cell are the same. However, in practical operation, the relevant parameters of different devices, such as ON-resistance, state voltage drop, and the thermal expansion coefficients of the material are diverse. Furthermore, replacing damaged modular units after failure also inevitably leads to aging mismatches among the power modules, which can be shown in Fig. 2. Therefore, designing an effective strategy to alleviate the aging mismatch problem in a modular system has become a significant research problem in the field of power electronics technology [17]. In [17], the aging process of the interleaved boost dc–dc conversion system is studied, and a method that can easily manage the power distribution of system cells is proposed. On the other hand, considering the failure mechanism of sensitive cells in the system, in [26], an approach is proposed to delay the occurrence of system failure, thereby increasing the system lifetime.

In any case, the topic of the lifetime extension for the power electronic systems needs further research based on the following.

1) Application of data-based approaches for the problem of alleviating aging degree mismatch in the modular power conversion system.
2) Limitation of the conventional model-based approaches to estimate the SOH of the system without recognizing the accurate mathematical model.

To face these difficulties, this article proposes a novel lifetime extension approach for interleaved dc–dc boost conversion systems based on the Levenberg–Marquardt back propagation neural network (LM-BPNN) and power routing strategy. The main contributions of this article can be summarized as follows.

1) Without prior knowledge and a mathematical model, a data-based health state estimation approach is proposed to overcome the shortcomings of model-based approaches, which can effectively estimate the SOH in real time.
2) Considering the proposed SOH estimation, a power routing strategy is applied to allocate different power to each power cell in the system with the aid of the data-based cumulated damage estimation approach. In this sense, the power distribution can be optimized, and the problem of aging mismatch is alleviated.
3) Numerical simulation results show that the proposed lifetime extension approach can extend the overall system lifetime. Furthermore, an experimental setup of the interleaved dc–dc boost conversion is constructed to verify the proposed approach.

The rest of this article is organized as follows. Section II states the research problem. Section III illustrates the lifetime extension approach based on the LM-BPNN and power routing strategy. Section IV uses a numerical simulation to verify the proposed approach. Section V constructs an experimental setup of the interleaved dc–dc boost conversion to verify the proposed lifetime extension approach. Finally, Section VI concludes this article.

II. Problem Statement

This article aims to estimate the SOH of an interleaved dc–dc boost conversion system with the aid of a data-based approach. Furthermore, the problem of mismatched aging in the system is alleviated, and the overall system lifetime can be extended. To facilitate discussion, the complete Vensys 60/1200 system shown in Fig. 1 can be simplified into the form of an interleaved dc–dc boost conversion system, as shown in Fig. 3. The diode rectifier bridge and the active front end are assumed to be equivalent to the voltage sources V_d and V_o, respectively.

The SOH estimation approach proposed in this article is based on the historical data generated by the system during the operational process. It is supposed that the data in the ith working cycle can be expressed as $x(i) = [x_{(i,1)}, x_{(i,2)}, \ldots, x_{(i,p)}]$, where p is the number of sensors. Correspondingly, the true

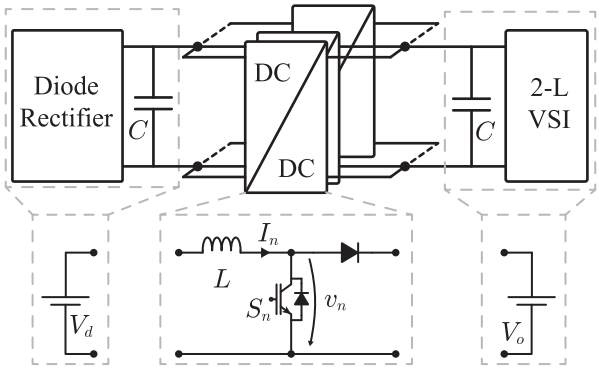

Fig. 3. Simplified structure of the Vensys 60/1200 system.

value of the systematic SOH under the current cycle is $y(i)$. The original dataset can be reconstructed by combining $x(i)$ and $y(i)$, which is expressed as $D = \{(x(i), y(i))|i = 1, 2, \ldots, m\}$, where m is the total number of samples. On this basis, the SOH estimation approach proposed in this article takes the historical data (training data) as the input of the data-based learning algorithm model. The best mapping function $\Phi : x(i) \rightarrow y(i)$ is learned by training the model. Furthermore, based on the trained algorithm model and online working data, the real-time SOH estimation can be achieved.

Correspondingly, root mean square error (RMSE) and mean absolute error (MAE) are considered as indicators to evaluate the SOH estimation performance [27], [28]. The RMSE is defined as

$$\text{RMSE} = \sqrt{\frac{1}{n}\sum_{i=1}^{n}(\text{SOH}_{ei} - \text{SOH}_{ti})^2} \tag{1}$$

where n is the number of samples in the testing sets, i is the index of the samples, SOH_{ei} and SOH_{ti} are SOH estimated value and SOH ground truth of the ith testing sample, respectively. Furthermore, MAE is shown as follows:

$$\text{MAE} = \frac{1}{n}\sum_{i=1}^{n}|\text{SOH}_{ei} - \text{SOH}_{ti}|. \tag{2}$$

Equations (1) and (2) measure the difference between the SOH ground truth and the estimated value. The smaller the value, the better the SOH estimation performance of the algorithm model.

It should be noted that this article implements the health management of the power cells according to the SOH of each power cell in the dc–dc boost conversion system. Specifically, in order to evaluate the health status of the system, the cumulated damage of each cell is calculated as the SOH by the rainflow counting method according to the amplitude temperature $\triangle T$ and the average thermal cycle temperature $T_{j,m}$, which is widely adopted in power conversion systems [26]. The principle of the rainflow counting method is shown in Fig. 4, which can isolate the task profile of the temperature derivative change. The temperature transition from hot to cold is reflected. In addition, the temperature difference between the two operational points is calculated. On this basis, the number of thermal cycles to failure N_f can be acquired by the rainflow counting algorithm [26], as

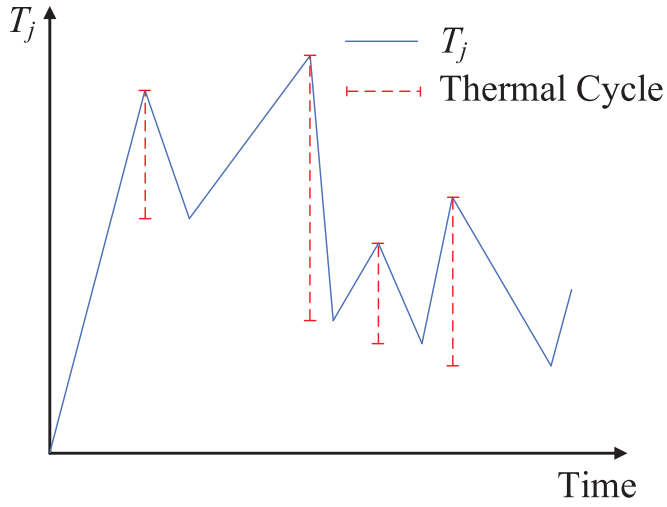

Fig. 4. Example of the rainflow algorithm.

follows:

$$N_f = \alpha\left(\triangle T\right)^{(-\beta)} e^{\frac{E_a}{k_B\left(T_{j,m}+273^\circ C\right)}} \tag{3}$$

where α and β are device dependent parameters, respectively. E_a is the excitation energy of the device material, and k_B is Boltzmann constant. On this basis, the cumulated damage D can be defined according to the Miner fatigue cumulative principle as follows:

$$D = \sum_i \frac{N_i}{N_{f_i}} \tag{4}$$

where N_i is the number of thermal cycles, and N_{f_i} is the maximum number of thermal cycles that the device can withstand. Through (3) and (4), the cumulated damage D is dependent on a history of the information, the junction temperature, and temperature changes, from the initial working point. Although the rainflow counting method can consider historical information, as shown in (3) and (4), it should be noted that only temperature information is considered. On the other hand, when using the machine learning algorithm, the mapping relationship between current, voltage, temperature, and cumulated damage at the current moment is constructed. Due to the more comprehensive feature information, the mapping relationship between input and cumulated damage can be constructed even without historical temperature information. In this sense, we attempt to adopt a neural network-based approach to construct the mapping relationship between current, voltage, temperature, and cumulated damage at the current moment in this article.

From a theoretical point of view, when the cumulated damage D becomes 1, it means that, on average, the power device will fail. But D represents a cumulated probabilistic measure of the failure. Depending on the application and how critical it is, the acceptable cumulated damage is different. For instance, in regular applications, the maximum value in the failure probability is 20%. As for aeronautical applications, this threshold is set from 0.1% to 1%. This article sets the maximum value of

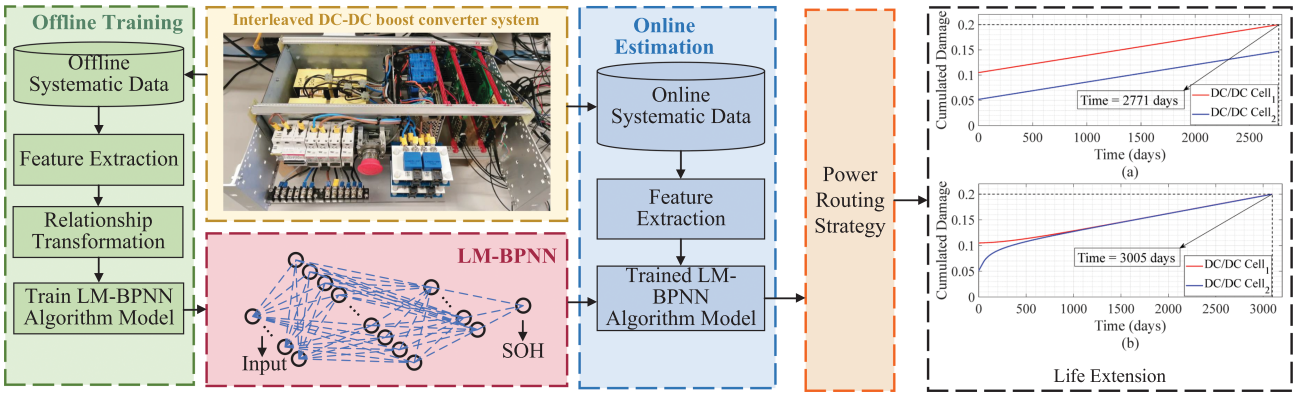

Fig. 5. Research flow.

the cumulated damage to 20%. When the cumulative damage reaches 20%, the power cell should be replaced.

III. Lifetime Extension Approach

The lifetime extension approach for interleaved dc–dc conversion systems proposed in this article is mainly composed of an LM-BPNN algorithm and a power routing strategy. The research flow of the approach is shown in Fig. 5. The LM-BPNN algorithm includes two parts: offline training and online estimation. For the offline training part, the feature variables, such as current, voltage, and temperature data generated by the dc–dc conversion system during the operation are extracted as the input of the LM-BPNN, and the cumulated damage at the corresponding time is the label. Afterward, the LM-BPNN is used to establish the mapping relationship between feature variables and cumulated damage. Regarding the power routing strategy, this part consists of a power routing control loop and a power module control loop. The power routing control loop takes the cumulated damage from the LM-BPNN as the input, and outputs the power sharing factor of each power cell in the dc–dc conversion system. The power module control loop is essentially an internal closed-loop control to track the desired per-cell power. According to the power sharing factor, the duty cycle of each dc–dc power cell is changed to fulfill the required power distribution, leading to achieving an equalization of the cumulated damage of all the power cells.

A. Levenberg–Marquardt Back Propagation Neural Network (LM-BPNN)

The BPNN has a strong self-adaptive learning ability, which completes the mapping from input to output by automatically learning the implicit relationship in the data [29], [30]. The gradient descent algorithm is generally used to update the weight parameters in the conventional BPNN [31]. The mean square error is used as the loss function to train the BPNN

$$F(\theta)=\frac{1}{2m}\sum_{i=1}^{m}\left(f_\theta(x_i)-y_i\right)^2 \tag{5}$$

where m is the number of samples in the training set, x_i and y_i are the input vector and the label of the ith sample, respectively. $f_\theta(x_i)$ is the estimated value of the network in the ith sample, and θ is the composition of the weight and the bias vector

$$\theta=\begin{bmatrix} w_{11} & w_{12} & \cdots & w_{1n} & b_1 \\ w_{21} & w_{22} & \cdots & w_{2n} & b_2 \\ \vdots & \vdots & \ddots & \vdots & \vdots \\ w_{n1} & w_{n2} & \cdots & w_{nn} & b_n \end{bmatrix} \tag{6}$$

where n is the dimension. However, the traditional gradient descent algorithm has disadvantages, such as low training efficiency and worse convergence. For this reason, this article introduces the LM algorithm to optimize the BPNN. The LM algorithm combines the advantages of the gradient descent and the Gauss–Newton algorithm. In detail, the LM algorithm can maintain the rapid convergence of the gradient descent algorithm, while having the optimal characteristics of the Gauss–Newton algorithm [32]. The training process of the BPNN can essentially be regarded as the solution to the minimum value of $F(\theta)$ for the nonlinear least-squares problem, as follows:

$$\min_{\theta\in R^n} F(\theta)=\frac{1}{2}\left(r(\theta)\right)^T r(\theta)=\frac{1}{2}\sum_{i=1}^{m}\left[r_i(\theta)\right]^2 (m\geq n) \tag{7}$$

where $r(\theta)$ is residual function of θ, which can be specifically shown as

$$r(\theta)=\left[r_1(\theta), r_2(\theta), \ldots, r_m(\theta)\right]^T. \tag{8}$$

It is assumed that $J_a(\theta)$ is the Jacobian matrix of $r(\theta)$, shown as follows:

$$\begin{aligned} J_a(\theta)&=\left[\nabla r_1(\theta), \nabla r_2(\theta), \ldots, \nabla r_m(\theta)\right]^T \\ &=\begin{bmatrix} \frac{\partial r_1}{\partial \theta_1} & \frac{\partial r_1}{\partial \theta_2} & \cdots & \frac{\partial r_1}{\partial \theta_n} \\ \frac{\partial r_2}{\partial \theta_1} & \frac{\partial r_2}{\partial \theta_2} & \cdots & \frac{\partial r_2}{\partial \theta_n} \\ \vdots & \vdots & \ddots & \vdots \\ \frac{\partial r_m}{\partial \theta_1} & \frac{\partial r_m}{\partial \theta_2} & \cdots & \frac{\partial r_m}{\partial \theta_n} \end{bmatrix}. \end{aligned} \tag{9}$$

The gradient $g(\theta)$ of $F(\theta)$ can be expressed as

$$g(\theta)=\sum_{i=1}^{m} r_i(\theta)\nabla r_i(\theta)=\left(J_a(\theta)\right)^T r(\theta). \tag{10}$$

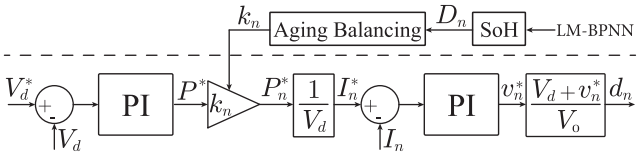

Fig. 6. Power routing strategy structure.

It should be noted that the LM algorithm is improved on the basis of the Gauss–Newton method, which changes the step size in the iteration. For the kth iteration, the gradient can be described by

$$\triangle_k = -\left[\left(J_a\left(\theta_k\right)\right)^T J_a\left(\theta_k\right) + u_k I\right]^{-1} \left(J_a\left(\theta_k\right)\right)^T r\left(\theta_k\right) \tag{11}$$

where u_k is the penalty factor, and I is the unit matrix. When the value of u_k is large, the LM algorithm is equivalent to the gradient descent algorithm, because the elements on the main diagonal occupy a dominant position. On the other hand, when the value of u_k is small, the LM algorithm is equivalent to the Gauss–Newton method. The details about LM-BPNN can be referred to [32].

In general, larger u_k is used in the initial stage of the training process to accelerate the convergence of the network. In the later stage of the training process, smaller u_k is used to avoid the oscillations generated by the gradient descent algorithm so that the network can be converted to the global optimal solution as much as possible. In this sense, the cumulated damage can be accurately estimated.

B. Power Routing Strategy

The power routing strategy structure of the interleaved dc–dc boost conversion system is shown in Fig. 6 [17]. The essence of the power routing strategy is to allocate different power to corresponding power cells by adjusting the transient current through the inductor according to the actual situation of the cumulated damage.

The power routing strategy of the interleaved dc–dc power system consists of a power routing control loop and an internal power module control loop.

1) Power Routing Control Loop: The cumulated damage obtained in the LM-BPNN is taken as the input in the power routing control loop. The output is the power sharing factor of each cell in the dc–dc conversion through specific distribution rules that will be introduced later. In this article, the cumulated damage of each power cell is used as the SOH to measure its health status. The damage of the power device is closely related to its temperature and the suffered cycles thermal amplitudes. In this sense, the greater power managed by a power cell will increase its temperature, leading to accelerating the aging of the corresponding power devices. Therefore, to balance the aging of all power devices as much as possible, the purpose of the power routing control loop is to allocate lower power to cells with higher cumulated damage and allocate higher power to cells with lower cumulated damage.

The parameter k_i in Fig. 6 is the power sharing factor of the ith power cell, which determines the actual power to be managed by each cell. To ensure the normal operation of the system, it is worth noting that whatever the power distribution inside the system is, the sum of the power sharing factors of all cells should be equal to 1, which can be expressed as

$$\sum_{i=1}^{q} k_i = 1 \tag{12}$$

where q is the number of cells in the system. Considering a conventional operation of an interleaved dc–dc boost system, the power sharing factors of all the power cells are equal

$$k_1 = k_2 = \cdots = k_i = \cdots = k_q = \frac{1}{q}. \tag{13}$$

To allocate different power to each cell, it is assumed that the cumulated damage of the ith cell is D_i. The value of the ith cell power sharing factor k_i can be expressed as

$$k_i = \frac{\sum_{j=1}^{q} D_j^{\gamma} - D_i^{\gamma}}{(q-1)\sum_{j=1}^{q} D_j^{\gamma}} \tag{14}$$

where γ is an exponential term, which aims to increase the difference between the cumulated damage of different cells to speed up the power equalization by making the power routing method more robust. In particular, when the damage of all cells is the same, (14) achieves the equalized operation described in (13), leading to the conventional interleaved operation of the power system.

2) Internal Power Module Control Loop: The power module control loop is essentially a closed-loop control with a power tracking objective, as shown in Fig. 6. According to the power sharing factors calculated by the power routing control method, the duty cycle of each cell is determined to complete the objective of power distribution. The control scheme presented in [17] is widely used in the interleaved parallel power modules. For the ith power cell, the closed-loop control determines the power P_i^* to be managed by the ith power cell by using the power sharing factor, and divides it by the input voltage V_d to obtain the reference current I_i^* that has to flow through the inductor. Afterward, the reference inductor voltage v_i^* can be determined through an internal control loop implemented with another PI controller. Finally, by means of normalization, the duty cycle d_i to generate the gate driving pulse (S_i) of each module is obtained by applying a simple pulsewidth modulation method.

IV. Numerical Simulation Analysis

A. Systematic Introduction

To test the proposed lifetime extension approach, this article uses a two-cell interleaved dc–dc boost conversion system for numerical simulation analysis. The structure diagram of the system is shown in Fig. 3. The power device used in the conversion system is the IRFP4227 MOSFET. Moreover, the relevant parameters of the system are summarized in Table I. Both dc–dc power cells are connected to an input power source and an output capacitor. All the experiments are performed at an ambient temperature equal to 40 °C.

Based on the parameter configuration listed in Table I, the power curve of the dc–dc boost conversion system ranges from

TABLE I
PARAMETERS IN THE DC–DC BOOST CONVERTER SYSTEM

Parameter	Value
Number of cells	2
Input voltage (V)	50
Output voltage (V)	140
Switching frequency (kHz)	5
Boost inductance (mH)	3
Ambient temperature (°C)	40

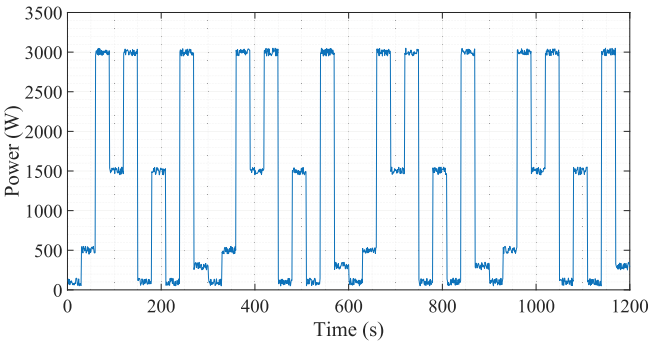

Fig. 7. Power profile applied to the complete DC–DC power system.

0 to 3 kW, whose value is accompanied by a certain random disturbance. The specific 20-min power profile is shown in Fig. 7. It should be noted that the power profile represented in Fig. 7 is repeated to form complete days. On the basis of the parameter configuration and operating power described previously, the cumulated damage of each power cell in the dc–dc boost conversion system is obtained by the rainflow counting method [33].

B. Cumulated Damage Estimation Based on the LM-BPNN

In the interleaved dc–dc boost conversion system, the whole simulation time of an operational process is set to one year. For each simulation cycle, namely, each day, feature variables, such as the current, voltage, and temperature of the power device are extracted as the input of the LM-BPNN model. Correspondingly, the output of the LM-BPNN is the cumulated damage at the end of the day. It should be noted that the cumulated damage is calculated according to the rainflow counting method in (3) and (4) for each day, which is used as the label of the training data.

To simulate various unbalanced initial aging scenarios, the initial damages are randomly assigned to the two cells in the dc–dc boost conversion system. The data from multiple operational conditions can be obtained to verify the effectiveness of the LM-BPNN estimation algorithm proposed in this article. The ratio of training data to test data is set to 5:1 in this article. In detail, the data of 30 operational processes are used as training data, and the data of six operational processes are used as testing data to verify the estimation performance. To prevent overfitting in the training process, this article adopts the tenfold cross-validation method to adjust parameters, such as the network learning rate and the number of network neurons, to acquire a great cumulative damage estimation performance. The details of the tenfold cross validation are shown in Fig. 8.

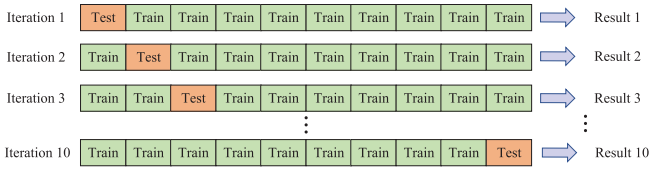

Fig. 8. Tenfold cross validation.

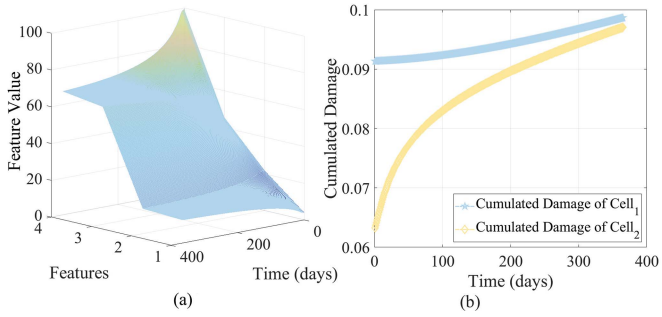

Fig. 9. Visualization of features and cumulated damage.

TABLE II
ESTIMATION RESULTS OF THE TWO POWER CELLS USING TENFOLD CROSS VALIDATION

Configuration	Parameter	$Cell_1$		$Cell_2$	
		RMSE	MAE	RMSE	MAE
1	(16,16)	9.293×10^{-5}	8.856×10^{-5}	1.789×10^{-4}	1.334×10^{-4}
2	(16,32)	$\mathbf{2.782 \times 10^{-5}}$	$\mathbf{2.220 \times 10^{-5}}$	$\mathbf{4.006 \times 10^{-5}}$	$\mathbf{2.138 \times 10^{-5}}$
3	(16,64)	1.258×10^{-4}	9.372×10^{-5}	1.386×10^{-4}	8.562×10^{-5}
4	(32,16)	4.983×10^{-5}	4.596×10^{-5}	8.359×10^{-5}	6.968×10^{-5}
5	(32,32)	1.454×10^{-4}	1.128×10^{-4}	2.364×10^{-4}	1.512×10^{-4}
6	(32,64)	3.589×10^{-3}	3.141×10^{-4}	6.798×10^{-3}	4.485×10^{-4}
7	(64,16)	7.025×10^{-4}	6.858×10^{-4}	1.783×10^{-3}	1.052×10^{-3}
8	(64,32)	1.751×10^{-3}	8.992×10^{-4}	1.963×10^{-3}	1.616×10^{-3}
9	(64,64)	6.896×10^{-3}	6.334×10^{-4}	5.038×10^{-3}	3.856×10^{-3}

In detail, the training dataset is divided into ten parts, each part of which is used as test data for verification in turn, and nine of them are used as training data for model training. The average of the ten experiments measures the final indicator.

To better demonstrate the influence of features on the cumulated damage, this work uses four features, namely, the current and temperature of two cells of the interleaved dc–dc boost conversion system in an operational process [see an example to visualize the features in Fig. 9(a)]. Furthermore, the corresponding cumulated damage is shown in Fig. 9(b). It can be seen from Fig. 9 that there is a correlation between the current, temperature features of the two cells, and the cumulated damage, which also provides the feasibility of constructing the mapping relationship between the characteristics and the cumulated damage in this work.

Considering that the amount of data collected in the parallel dc–dc boost conversion system is small, the number of layers of the network is set to two. On this basis, a grid search is performed in a two-layer network to determine the number of neurons in each layer so that a better cumulated damage estimation performance can be obtained. In detail, the possible values of the number of neurons in the two-layer network are set to 16, 32, and 64. Table II lists the results of the RMSE

TABLE III
HYPERPARAMETER CONFIGURATION

Hyperparameter	Value
Number of layers	2
Number of neurons	(16,32)
Learning rate	0.001
Epoch	1000
Activation function	tanh

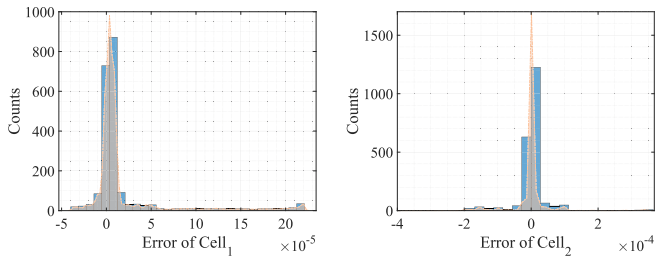

Fig. 10. Error distribution of the two power cells.

and MAE of the two power cells of the dc–dc boost conversion system under multiple network configurations using tenfold cross validation. When the number of neurons in the two-layer network is 16 and 32, respectively, the LM-BPNN has a better estimation performance. The hyperparameter configuration of the LM-BPNN is summarized in Table III.

To better demonstrate the estimation performance of the proposed approach on the testing dataset, the error distribution of the two power cells of the dc–dc boost conversion system in the testing data under multiple network configurations is represented, which is shown in Fig. 10. It can be seen from Fig. 10 that the error of the two power cells is mainly distributed on both sides of zero, which is concentrated in the order of magnitude of 10^{-5}. It can also confirm that the proposed approach has a great cumulative damage estimation performance.

To demonstrate the cumulated damage estimation performance of the proposed LM-BPNN, this article represents the cumulated damage estimation results of the LM-BPNN in the six operational processes of the testing data, shown in Fig. 11. It should be noted that the training data and testing data in the article are performed under the power routing strategy, and the power profile applied to the system is consistent with Fig. 6. It can be seen that the estimated cumulated damage curve coincides nicely with the actual cumulative damage curve, which represents that the estimation performance of the LM-BPNN is excellent. Table IV lists the results of the RMSE and MAE of the testing data in the cumulated damage estimation of these six operational processes.

To demonstrate the superiority of the approach proposed in this article, the Cell_2 of the first operational process, whose initial damage is 0.052, is used as an example to compare the estimation performance of the LM-BPNN and other data-based estimation approaches, such as ridge regression (Ridge), support vector regression (SVR), ElasticNet regression (ElasticNet), Lasso regression (Lasso), AdaBoost regression (AdaBoost), k-Nearest Neighbor (KNN), partial least squares regression (PLS), and long-short term memory network (LSTM). Fig. 12 represents the estimation results of various methods on the testing data. From Fig. 12, it can be seen that the estimated cumulated damage of the proposed LM-BPNN is the closest to the ground truth. Correspondingly, the evaluation indicators are shown in Table V. It can be seen from Fig. 12 and Table V that the LM-BPNN proposed in this article has the best estimated performance on cumulated damage compared with other data-based estimation approaches. Although the uncertainty for unit heterogeneity may cause slight errors between the estimated damage and the ground truth, it is acceptable from the results. The reason is that the SOH can be reflected through the feature variables of each power cell. Therefore, the machine learning algorithm is considered to construct a mapping relationship between current, voltage, temperature, and cumulated damage, which can acquire excellent estimation performance.

TABLE IV
ESTIMATION RESULTS OF CUMULATED DAMAGE

Operational number	Cell	Initial Damage	RMSE	MAE
1	Cell_1	0.105	3.348×10^{-6}	2.386×10^{-6}
	Cell_2	0.052	1.835×10^{-5}	4.301×10^{-6}
2	Cell_1	0.124	8.350×10^{-6}	6.081×10^{-6}
	Cell_2	0.032	2.908×10^{-5}	1.162×10^{-5}
3	Cell_1	0.153	1.239×10^{-4}	1.004×10^{-4}
	Cell_2	0.063	1.205×10^{-4}	8.024×10^{-5}
4	Cell_1	0.083	8.920×10^{-6}	8.335×10^{-6}
	Cell_2	0.032	1.237×10^{-5}	8.924×10^{-6}
5	Cell_1	0.073	5.011×10^{-6}	3.929×10^{-6}
	Cell_2	0.022	9.320×10^{-6}	5.025×10^{-6}
6	Cell_1	0.108	1.744×10^{-5}	1.200×10^{-5}
	Cell_2	0.010	5.075×10^{-5}	1.819×10^{-5}

C. Simulation Results of the Power Routing Strategy

To represent the lifetime extension performance of the power routing strategy on the interleaved dc–dc boost conversion system, this article shows the cumulated damage before and after the introduction of the power routing strategy. Specifically, for the first operation in the testing data, the initial damages of the two power cells in the system are set to 0.105 and 0.052, respectively. It should be noted that the maximum power sharing factor is set to 0.8 so that an excessive power mismatch among the cells is avoided. The cumulated damage value, cumulated damage difference, and power sharing factor of the two cells are plotted in Fig. 13.

According to the power routing strategy, since the initial damages of the two cells in the interleaved dc–dc boost conversion system are different, the two cells will have different power sharing factors to manage different power in each cell. It can be seen from Fig. 13 that the cumulated damage difference between the two cells in the system is continuously reduced by applying the power routing strategy. The damage growth of cells with higher cumulated damage will be significantly slower than the cells with lower cumulated damage to delay the failure of cells with a higher cumulated damage and to extend the overall system lifetime. The numerical simulation result represents that

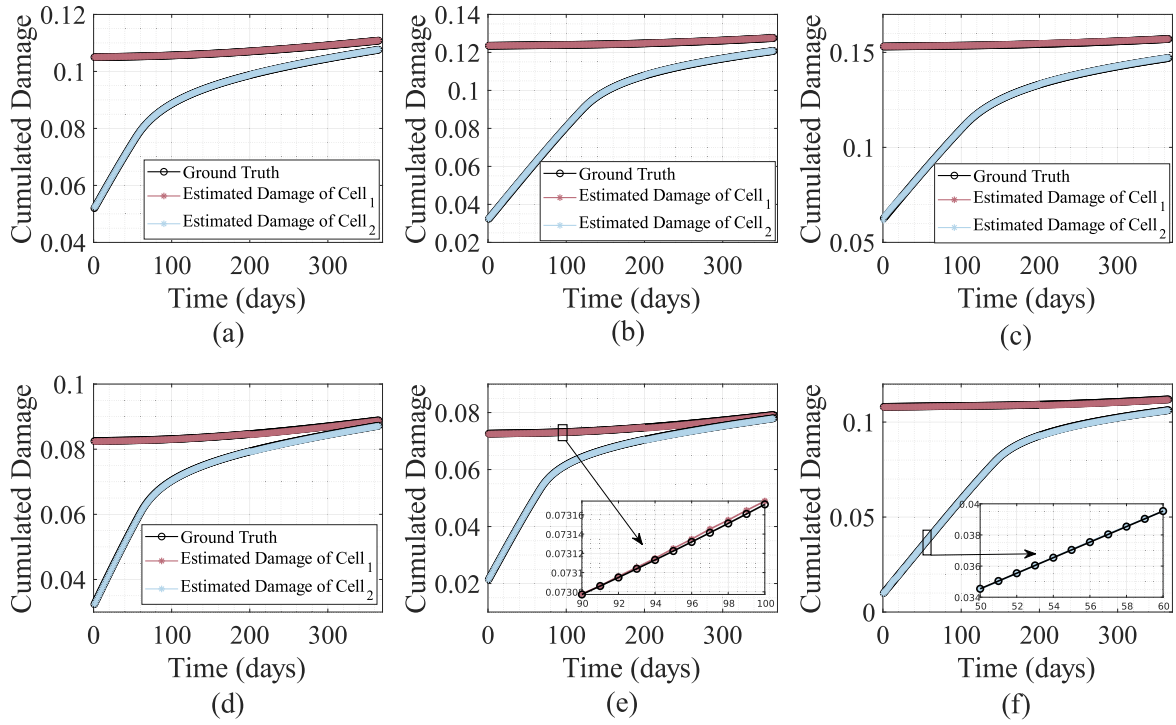

Fig. 11. Estimation results of the LM-BPNN in the six operational processes of the testing data.

TABLE V
COMPARISON OF THE CUMULATED DAMAGE ESTIMATION RESULTS USING DIFFERENT APPROACHES

Approach	Ridge	SVR	ElasticNet	Lasso	AdaBoost	KNN	PLS	LSTM	LM-BPNN
RMSE	4.433×10^{-3}	2.373×10^{-2}	2.186×10^{-2}	1.793×10^{-2}	7.448×10^{-3}	5.606×10^{-3}	3.527×10^{-3}	3.222×10^{-3}	$\mathbf{1.835 \times 10^{-5}}$
MAE	3.824×10^{-3}	2.192×10^{-2}	1.985×10^{-2}	1.641×10^{-2}	6.646×10^{-3}	4.552×10^{-3}	2.793×10^{-3}	2.580×10^{-3}	$\mathbf{4.301 \times 10^{-6}}$

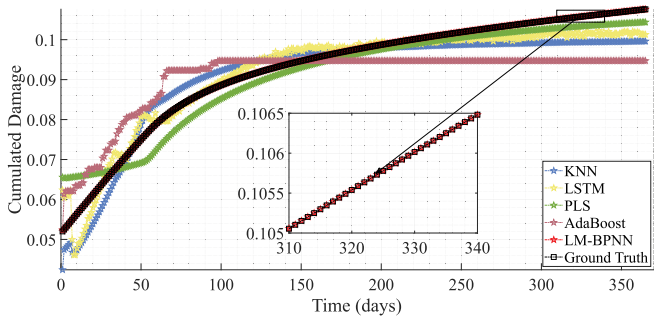

Fig. 12. Estimation results of the cumulated damage using different data-based approaches.

TABLE VI
PARAMETERS IN THE DC–DC BOOST CONVERTER SYSTEM

Parameter	Value
Number of cells	2
Input voltage (V)	50
Output voltage (V)	140
Switching frequency (kHz)	4
Boost inductance (mH)	3
Output capacitor (mF)	5.6
Load resistor (Ω)	44
Ambient temperature (°C)	25

the lifetime of the system without the power routing strategy and under the power routing strategy is 2771 days and 3005 days, respectively, from which the effectiveness of the proposed lifetime extension approach can be verified. It is worth mentioning that the principle of neural network training is consistent when faced with a dc–dc conversion system that contains more cells. The feature variables, such as the current, voltage, and temperature of each cell are extracted as the input of the LM-BPNN model so that the cumulated damage estimation can be achieved. In this sense, the life extension approach proposed in this article has great scalability. The reason is that the principle is consistent.

V. EXPERIMENTAL SETUP

To verify the lifetime extension approach, an experimental setup of the interleaved dc–dc boost conversion is constructed, shown in Fig. 14. For each boost module, the power device is a 200-V MOSFET IRFP4227PbF from Infineon Technologies. Furthermore, these two dc–dc converters are connected to input power. The output is a parallel circuit of a resistor and a capacitor. The interleaved dc–dc boost conversion system is controlled by DS1004 from the DSpace solution. The interleaved modulation, data acquisition, and control scheme are implemented in the DSpace platform. In detail, the parameters in the dc–dc boost conversion system are summarized in Table VI. In addition, the

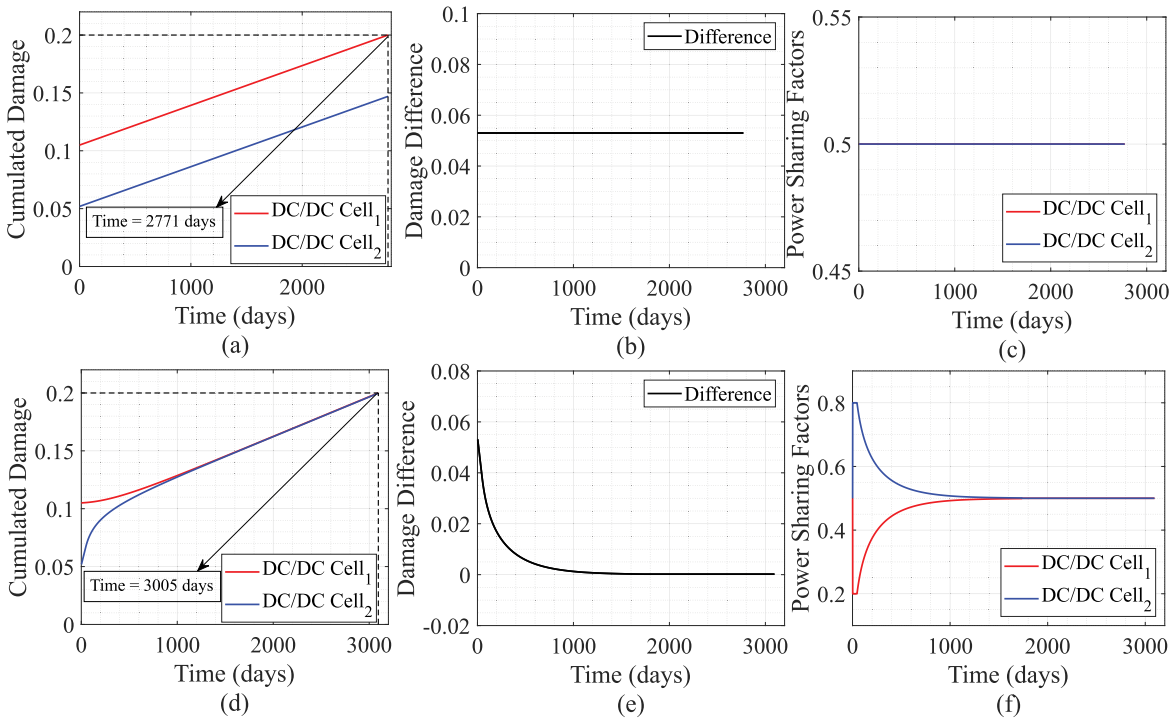

Fig. 13. Simulation results of the power routing strategy. (a)–(c) Cumulated damage, cumulated damage difference, and power sharing factor of the system without the power routing strategy. (d)–(f) Cumulated damage, cumulated damage difference, and power sharing factor of the system under the power routing strategy.

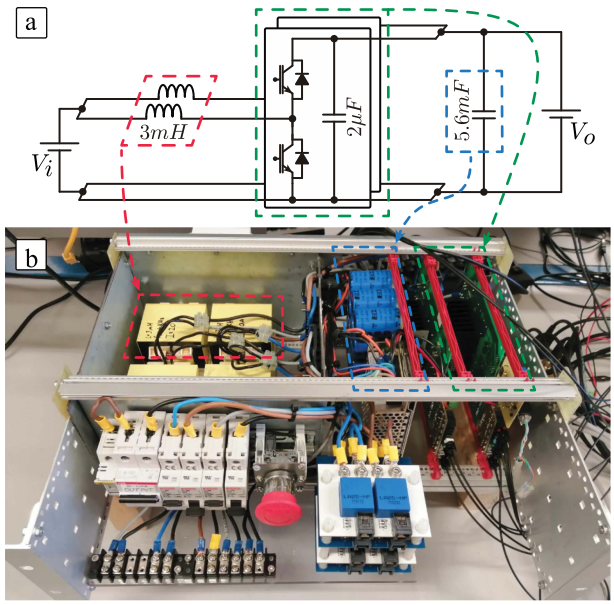

Fig. 14. Experimental setup. (a) Circuit configuration. (b) Experimental platform.

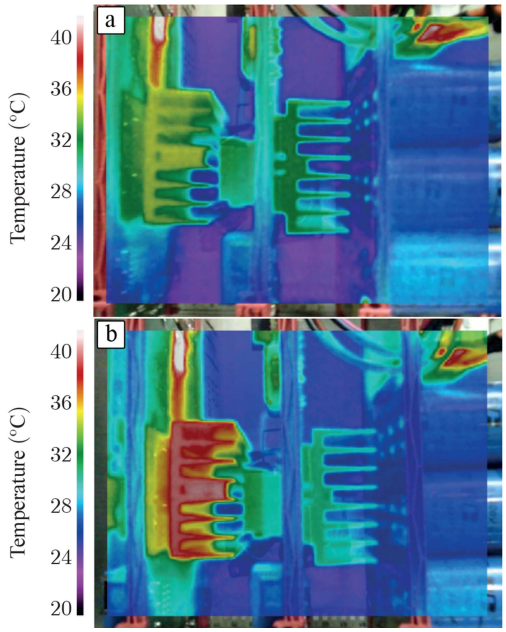

Fig. 15. Temperature measurement module of experimental setup. (a) Temperature without applying the power routing method. (b) Temperature applying the power routing method.

temperature of the power module is measured by a data logging interface of the thermocouple, shown in Fig. 15.

In the offline training preparation stage of the experiment, the two converter cells just shipped in the dc–dc boost converter system are arranged in a symmetrical manner. Under this condition, the initial cumulated damage of both converter cells is zero. In order to simulate the aging mismatch between the power modules, different power factor weights, as described in (14), are set by the DSpace controller, thereby distributing different powers to the two converter cells. It is worth mentioning that no power routing strategy is used in the aforementioned process, thus different cumulated damages are obtained. In this

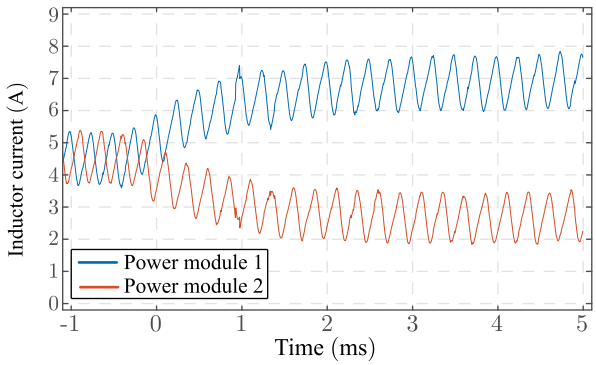

Fig. 16. Inductor currents of the two modules. The power routing method is enabled at $t = 0$.

sense, the power control strategy is changed after the system works for a period of time. In other words, when the power routing strategy is adopted, the two converter cells have different initial cumulated damages. In this process, according to the temperature measurement module of the experimental setup in Fig. 15, the temperature of the two converter units can be measured in real time. In this sense, the cumulated damage of the two converter cells can be calculated in real time by the rainflow counting method described by (3) and (4). On the other hand, the corresponding voltage, current, and temperature data can be saved as offline training data. By repeating the aforementioned process, the current, voltage, and temperature data required for offline training of the neural network, and the cumulated damage labels at the corresponding time can be obtained, thereby completing the training of the neural network. In the aforementioned process, it is not necessary to use the initial cumulated damage for the training of the neural network. The reason is that the corresponding cumulated damage is calculated on a freshly shipped converter unit. Initial damage does not have to be considered during the training process.

It is supposed that dc–dc Cell_2 has higher cumulated damage than dc–dc Cell_1. On this basis, the proposed lifetime extension approach is applied to alleviate the aging mismatch problem in the modular system of the experimental setup. Based on the trained offline LM-BPNN in (5)–(11), the real-time cumulated damage estimation is accomplished through the current, voltage, and temperature data collected online. Furthermore, the power routing control loop takes the estimated cumulated damage determining the power sharing factor of each power cell in the dc–dc conversion system by applying (12)–(14). In this way, the duty cycle of each dc–dc power cell is changed to complete the power distribution with the aid of the control loop. To demonstrate the control performance of the power routing strategy, Fig. 16 represents the current of both power modules. Whereas the different cumulated damage, under the premise that the total power remains unchanged, the two modules are given different average inductor currents, 6.9 A (dc–dc Cell_1) and 2.7 A (dc–dc Cell_2), respectively. In this sense, the cumulated damage difference between the two modules is reduced, to alleviate the aging mismatch problem.

VI. Conclusion

A lifetime extension approach for the interleaved dc–dc boost conversion system based on the LM-BPNN and power routing strategy is proposed in this article. According to the actual situation of the cumulated damage, the interleaved dc–dc boost conversion system allocates different power to the cells under the power routing strategy, thereby effectively extending the overall system lifetime. The main contributions of this article can be summarized in the following aspects.

1) Power routing strategy is applied to allocate different power to the power cells according to cumulated damage with the aid of the data-based cumulated damage estimation approach, to delay the arrival of the system failure.
2) A data-based health state estimation approach is proposed to overcome the shortcomings of model-based approaches.
3) A numerical simulation and an experimental validation of the interleaved dc–dc boost conversion are shown to verify the proposed approach, which alleviates the aging mismatch problem. To better apply the approach to the practical industrial process, a DSP platform is considered for the application of the proposed lifetime extension approach in future research.

References

[1] R. Wang, H. Xiao, L. Zhou, and M. Cheng, "An improved zero-voltage-transition h6-type transformerless grid-connected inverter with reactive power capability," *IEEE Trans. Power Electron.*, vol. 37, no. 2, pp. 2297–2306, Feb. 2022.

[2] S. Pugliese, M. Andresen, R. A. Mastromauro, G. Buticchi, S. Stasi, and M. Liserre, "A new voltage balancing technique for a three-stage modular smart transformer interfacing a dc multibus," *IEEE Trans. Power Electron.*, vol. 34, no. 3, pp. 2829–2840, Mar. 2019.

[3] J. I. Leon, S. Kouro, L. G. Franquelo, J. Rodriguez, and B. Wu, "The essential role and the continuous evolution of modulation techniques for voltage-source inverters in the past, present, and future power electronics," *IEEE Trans. Ind. Electron.*, vol. 63, no. 5, pp. 2688–2701, May 2016.

[4] J. I. Leon, S. Vazquez, and L. G. Franquelo, "Multilevel converters: Control and modulation techniques for their operation and industrial applications," *Proc. IEEE*, vol. 105, no. 11, pp. 2066–2081, Nov. 2017.

[5] V. G. Monopoli et al., "Applications and modulation methods for modular converters enabling unequal cell power sharing: Carrier variable-angle phase-displacement modulation methods," *IEEE Ind. Electron. Mag.*, vol. 16, no. 1, pp. 19–30, Mar. 2022.

[6] S. Vazquez, P. Acuna, R. P. Aguilera, J. Pou, J. I. Leon, and L. G. Franquelo, "DC-link voltage-balancing strategy based on optimal switching sequence model predictive control for single-phase H-NPC converters," *IEEE Trans. Ind. Electron.*, vol. 67, no. 9, pp. 7410–7420, Sep. 2020.

[7] Y. Yin et al., "Observer-based adaptive sliding mode control of NPC converters: An RBF neural network approach," *IEEE Trans. Power Electron.*, vol. 34, no. 4, pp. 3831–3841, Apr. 2019.

[8] S. Stynski, W. Luo, A. Chub, L. G. Franquelo, M. Malinowski, and D. Vinnikov, "Utility-scale energy storage systems: Converters and control," *IEEE Ind. Electron. Mag.*, vol. 14, no. 4, pp. 32–52, Dec. 2020.

[9] F. Cecati, R. Zhu, M. Liserre, and X. Wang, "Nonlinear modular state-space modeling of power-electronics-based power systems," *IEEE Trans. Power Electron.*, vol. 37, no. 5, pp. 6102–6115, May 2022.

[10] V. G. Monopoli, A. Marquez, J. I. Leon, Y. Ko, G. Buticchi, and M. Liserre, "Improved harmonic performance of cascaded h-bridge converters with thermal control," *IEEE Trans. Ind. Electron.*, vol. 66, no. 7, pp. 4982–4991, Jul. 2019.

[11] W. Luo, S. Stynski, A. Chub, L. G. Franquelo, M. Malinowski, and D. Vinnikov, "Utility-scale energy storage systems: A comprehensive review of their applications, challenges, and future directions," *IEEE Ind. Electron. Mag.*, vol. 15, no. 4, pp. 17–27, Dec. 2021.

[12] S. Vazquez, E. Zafra, R. P. Aguilera, T. Geyer, J. I. Leon, and L. G. Franquelo, "Prediction model with harmonic load current components for FCS-MPC of an uninterruptible power supply," *IEEE Trans. Power Electron.*, vol. 37, no. 1, pp. 322–331, Jan. 2022.
[13] M. Liserre et al., "Power routing: A new paradigm for maintenance scheduling," *IEEE Ind. Electron. Mag.*, vol. 14, no. 3, pp. 33–45, Sep. 2020.
[14] S. Rivera, S. Kouro, S. Vazquez, S. M. Goetz, R. Lizana, and E. Romero-Cadaval, "Electric vehicle charging infrastructure–from grid to battery," *IEEE Ind. Electron. Mag.*, vol. 15, no. 2, pp. 37–51, Jun. 2021.
[15] A. M. Alcaide et al., "Variable-angle PS-PWM technique for multilevel cascaded H-bridge converters with large number of power cells," *IEEE Trans. Ind. Electron.*, vol. 68, no. 8, pp. 6773–6783, Aug. 2021.
[16] P. R. Bana, K. P. Panda, and G. Panda, "Power quality performance evaluation of multilevel inverter with reduced switching devices and minimum standing voltage," *IEEE Trans. Ind. Inform.*, vol. 16, no. 8, pp. 5009–5022, Aug. 2020.
[17] A. Marquez et al., "Power devices aging equalization of interleaved DC–DC boost converters via power routing," *IEEE J. Emerg. Sel. Topics Ind. Electron.*, vol. 1, no. 1, pp. 91–101, Jul. 2020.
[18] J. Zhang, Y. Jiang, S. Wu, X. Li, H. Luo, and S. Yin, "Prediction of remaining useful life based on bidirectional gated recurrent unit with temporal self-attention mechanism," *Rel. Eng. Syst. Saf.*, vol. 221, 2022, Art. no. 108297.
[19] J. Tian, Y. Jiang, J. Zhang, Z. Wang, J. J. Rodríguez-Andina, and H. Luo, "High-performance fault classification based on feature importance ranking-XgBoost approach with feature selection of redundant sensor data," *Curr. Chin. Sci.*, vol. 2, no. 3, pp. 243–251, 2022.
[20] J. Zhang, X. Li, J. Tian, Y. Jiang, H. Luo, and S. Yin, "A variational local weighted deep sub-domain adaptation network for remaining useful life prediction facing cross-domain condition," *Rel. Eng. Syst. Saf.*, 2022, Art. no. 108986.
[21] M. Andresen, K. Ma, G. Buticchi, J. Falck, F. Blaabjerg, and M. Liserre, "Junction temperature control for more reliable power electronics," *IEEE Trans. Power Electron.*, vol. 33, no. 1, pp. 765–776, Jan. 2018.
[22] A. Al-Mohamad, G. Hoblos, and V. Puig, "A model-based prognostics approach for RUL forecasting of a degraded dc-dc converter," *4th Conf. Control Fault Tolerant Syst.*, 2019, pp. 312–318.
[23] S. Zhao, F. Blaabjerg, and H. Wang, "An overview of artificial intelligence applications for power electronics," *IEEE Trans. Power Electron.*, vol. 36, no. 4, pp. 4633–4658, Apr. 2021.
[24] D. Chiozzi, M. Bernardoni, N. Delmonte, and P. Cova, "A neural network based approach to simulate electrothermal device interaction in spice environment," *IEEE Trans. Power Electron.*, vol. 34, no. 5, pp. 4703–4710, May 2019.
[25] M. A. Eleffendi and C. M. Johnson, "In-service diagnostics for wire-bond lift-off and solder fatigue of power semiconductor packages," *IEEE Trans. Power Electron.*, vol. 32, no. 9, pp. 7187–7198, Sep. 2017.
[26] V. Raveendran, M. Andresen, and M. Liserre, "Improving onboard converter reliability for more electric aircraft with lifetime-based control," *IEEE Trans. Ind. Electron.*, vol. 66, no. 7, pp. 5787–5796, Jul. 2019.
[27] J. Zhang, Y. Jiang, X. Li, H. Luo, S. Yin, and O. Kaynak, "Remaining useful life prediction of lithium-ion battery with adaptive noise estimation and capacity regeneration detection," *IEEE/ASME Trans. Mechatronics*, vol. 28, no. 2, pp. 632–643, Apr. 2023.
[28] J. Zhang, Y. Jiang, X. Li, M. Huo, H. Luo, and S. Yin, "An adaptive remaining useful life prediction approach for single battery with unlabelled small sample data and parameter uncertainty," *Rel. Eng. Syst. Saf.*, vol. 222, 2022, Art. no. 108357.
[29] J. Zhang, K. Zhang, Y. An, H. Luo, and S. Yin, "An integrated multitasking intelligent bearing fault diagnosis scheme based on representation learning under imbalanced sample condition," *IEEE Trans. Neural Netw. Learn. Syst.*, early access, Jan. 6, 2023, doi: 10.1109/TNNLS.2022.3232147.
[30] J. Dong, W. Qin, and M. Wang, "Fast multi-objective optimization of multi-parameter antenna structures based on improved BPNN surrogate model," *IEEE Access*, vol. 7, pp. 77692–77701, 2019.
[31] J. Zhang et al., "A parallel hybrid neural network with integration of spatial and temporal features for remaining useful life prediction in prognostics," *IEEE Trans. Instrum. Meas.*, vol. 72, Dec. 2023, Art. no. 3501112, doi: 10.1109/TIM.2022.3227956.
[32] S. Wang, Y. Yuan, A. Zhou, and C. Yin, "Environmental study on analysis of characteristic parameters of rockfall movement based on field riprap test and establishment of SVM and LM-BPNN prediction models," *Ekoloji*, vol. 28, no. 107, pp. 3319–3326, 2019.
[33] V. Samavatian, H. Iman-Eini, and Y. Avenas, "An efficient online time-temperature-dependent creep-fatigue rainflow counting algorithm," *Int. J. Fatigue*, vol. 116, pp. 284–292, 2018.

Jiusi Zhang (Student Member, IEEE) received the B.E. degree in automation, in 2019, from Harbin Engineering University, Harbin, China, and the M.Sc. degree in control science and engineering, in 2021, from the Harbin Institute of Technology, Harbin, where he is currently working toward the Ph.D. degree in control science and engineering.

His research interests include fault diagnosis and prognosis, predictive maintenance, reliability and safety, prognostics and health management, and their applications in mechatronics and process industries.

Jilun Tian (Student Member, IEEE) received the B.E. degree in automation, in 2020, from Harbin Engineering University, Harbin, China, and the M.S. degree in control science and engineering, in 2022, from the Harbin Institute of Technology, Harbin, where he is currently working toward the Ph.D. degree in control science and engineering.

His research interests include the machine learning and its industrial applications in fault diagnosis, prognostics, and predictive maintenance.

Abraham M. Alcaide (Member, IEEE) was born in Huelva, Spain, in 1985. He received the B.S. and M.S. degrees in telecommunications engineering in 2014 and 2016, respectively, from the Universidad de Sevilla, Seville, Spain, where he is currently working toward the Ph.D. degree in electronic engineering.

His main research interests include modulation techniques, multilevel converters, power conversion for renewable energy sources, and model-based predictive control of power converters and drives.

Mr. Marquez was the recipient as co-author of the 2015 Best Paper Award of the IEEE INDUSTRIAL ELECTRONICS MAGAZINE.

Jose I. Leon (Fellow, IEEE) was born in Cádiz, Spain. He received the B.S., M.S., and Ph.D. degrees in telecommunications engineering from the Universidad de Sevilla, Seville, Spain, in 1999, 2001, and 2006, respectively.

He is currently an Associate Professor with the Department of Electronic Engineering, Universidad de Sevilla. Since 2019, he has also been the Chair Professor with the Department of Control Science and Engineering, Harbin Institute of Technology, Harbin, China. His research interests include modulation and control of power converters for high-power applications and renewable energy systems.

Dr. Leon was a co-recipient of the 2008 Best Paper Award of the IEEE INDUSTRIAL ELECTRONICS MAGAZINE, the 2012 Best Paper Award of the IEEE TRANSACTIONS ON INDUSTRIAL ELECTRONICS, and the 2015 Best Paper Award of the IEEE INDUSTRIAL ELECTRONICS MAGAZINE. He was the recipient of the 2014 IEEE J. David Irwin Industrial Electronics Society Early Career Award, the 2017 IEEE Bimal K. Bose Energy Systems Award, and the 2017 Manuel Losada Villasante Award for excellence in research and innovation.

Sergio Vazquez (Fellow, IEEE) was born in Seville, Spain, in 1974. He received the M.S. and Ph.D. degrees in industrial engineering from the University of Seville (US), Seville, in 2006 and 2010, respectively.

Since 2002, he has been with the Power Electronics Group working in R&D projects. He is currently an Associate Professor with the Department of Electronic Engineering, US. His research interests include power electronics systems, modeling, modulation, and control of power electronics converters applied to renewable energy technologies.

Dr. Vazquez was the recipient as a co-author of the 2012 Best Paper Award of theIEEE TRANSACTIONS ON INDUSTRIAL ELECTRONICS and the 2015 and 2022 Best Paper Award of the IEEE INDUSTRIAL ELECTRONICS MAGAZINE. He is involved in the Energy Storage Technical Committee of the IEEE Industrial Electronics Society and is currently serving as an Associate Editor for the IEEE TRANSACTIONS ON INDUSTRIAL ELECTRONICS.

Leopoldo G. Franquelo (Life Fellow, IEEE) was born in Málaga, Spain. He received the M.Sc. and Ph.D. degrees in electrical engineering from the Universidad de Sevilla, Seville, Spain, in 1977 and 1980, respectively.

From 1982 to 1986, he was an Associate Professor with the Department of Electronics Engineering, Universidad de Sevilla, where he has been a Professor since 1986. He has also been a 1000 Talent Professor with the Department of Control Science and Engineering, Harbin Institute of Technology, Harbin, China, since 2016. He has participated in more than 100 Industrial and R&D projects and has authored or co-authored more than 300 papers, 76 of them in IEEE Journals. His current research interests include modulation techniques for multilevel inverters and application to power electronic systems for renewable energy systems.

Dr. Franquelo has been a Distinguished Lecturer of the IEEE Industrial Electronics Society (IES) since 2006. In 2007, 2014, and 2016, he became an Associate Editor, Co-Editor-in-Chief, and the Editor-in-Chief of the IEEE TRANSACTIONS ON INDUSTRIAL ELECTRONICS. He was a Member-at-Large of the IEEE Industrial Electronics Society (IES) Administrative Committee (AdCom) from 2002 to 2003, the Vice President for Conferences from 2004 to 2007, and the President Elect of the IEEE IES from 2008 to 2009. He was the President of the IEEE IES from 2010 to 2011. He is a Life Member of the IEEE IES AdCom. In 2009 and 2013, he was the recipient of the prestigious Andalusian Research Award and the FAMA Award recognizing the excellence of his research career. He was also the recipient of a number of Best Paper Awards from IEEE journals. He was the recipient of the Eugene Mittelmann Outstanding Research Achievement Award and the Antohny J. Hornfeck Service Award from the IEEE IES, in 2012 and 2015, respectively.

Hao Luo (Senior Member, IEEE) received the B.E. degree in electrical engineering from Xi'an Jiaotong University, Xi'an, China, in 2007, and the M.Sc. and the Ph.D. degrees in electrical engineering and information technology from the University of Duisburg-Essen, Duisburg, Germany, in 2012 and 2016, respectively.

He is currently a Professor with the School of Astronautics, Harbin Institute of Technology, Harbin, China. His research interests include model-based and data-driven fault diagnosis, fault-tolerant systems, and their plug-and-play application on industrial systems.

Shen Yin (Fellow, IEEE) received the M.Sc. degree in control and information system and the Ph.D. (Dr.-Ing.) degree in electrical engineering and information technology from the University of Duisburg-Essen, Duisburg, Germany, in 2007 and 2012, respectively.

He is a DNV Endowed Full Professor with the Department of Mechanical and Industrial Engineering, Norwegian University of Science and Technology, Trondheim, Norway. His research interests include fault diagnosis/prognosis and fault-tolerance, reliability, safety, and security, data-driven monitoring and optimization, system and control theory, and applications on health diagnosis and cyber-physical systems.